Impact of the self-steepening effect on soliton spectral tunneling in PCF with three zero dispersion wavelengths

Hua Yang (杨 华)[1,2,*], Gangyan Xiao (肖港燕)[1], Saili Zhao (赵赛丽)[1], Zhixiang Tang (唐志祥)[1], Tao Li (李 涛)[1], Yupei Luo (罗誉培)[1], and Xue Tian (田 雪)[1]

[1]*College of Information Science and Engineering, Key Laboratory for Micro/Nano Optoelectronic Devices of Ministry of Education, Hunan University, Changsha 410082, China*

[2]*Synergetic Innovation Center for Quantum Effects and Application, Hunan Normal University, Changsha 410081, China*

**Corresponding author: huayang@hnu.edu.cn*

Received March 8, 2018; accepted May 8, 2018; posted online June 29, 2018

This work presents a numerical investigation of the self-steepening (SS) effect on the soliton spectral tunneling (SST) effect in a photonic crystal fiber (PCF) with three zero dispersion wavelengths. Interestingly, the spectral range and flatness can be flexibly tuned by adjusting the SS value. When the SS coefficient increases, the energy between solitons and dispersion waves is redistributed, and the red-shifted soliton forms earlier in the region of long wavelength anomalous dispersion. As a consequence, the SST becomes more obvious. The findings of this work provide interesting insights in regard to the impact of the SST effect on tailored supercontinuum generation.

OCIS codes: 060.5295, 190.4370.
doi: 10.3788/COL201816.070601.

The study on the mutual effect between optical solitons and dispersive waves (DWs) is one of the standing issues in the optical nonlinear area. It paves the way for validly regulating the peculiarity of supercontinuum generation (SCG)[1,2]. In general, solitons only exist in the anomalous dispersion region, where dispersion broadening can be balanced by nonlinear self-compression[3,4]. Nevertheless, a significant advance has been the realization that when an optical soliton, undergoing Raman-induced frequency shift (RIFS), approaches one of the zero dispersion wavelengths (ZDWs), it may be able to tunnel through a forbidden region of the normal group-velocity dispersion (GVD) between two anomalous dispersion regions and transfer its energy to a new soliton in the latter anomalous dispersion region[5,6]. This phenomenon shares a lot of similarities with the quantum mechanical tunneling across a latent barrier, thus named soliton spectral tunneling (SST)[7–9]. SST can shape not just the supercontinuum's (SC's) edge, but also shape its central part, which helps broadband SCG. The study of SST based on the nonlinear Schrödinger equation (NLSE) started with the pioneering research of Belyaeva and Serkin in 2001[10], since Newell predicted the tunneling effect existing in nonlinear media in 1978[11]. Then, subsequently, the effects of solitons tunneling governed by various NLSE were widely researched. For instance, in 2008, Wang *et al.* discussed the tunneling effects of a spectral component passing through a nonlinear optical barrier[12]. In the same year, Politti *et al.*[9] designed a number of realistic and simple holey fibers that are suitable for the observation of SST. In 2013, Guo *et al.*[8] indicated that the SST effect can be regarded as spectral coupling from an initial state to its eigenstate. In this progress, soliton self-frequency shift (SSFS) induced by a Raman response can balance the spectrum recoil effect; the launched soliton coupling continuously occurs until a new soliton appears in the adjacent channel. These works demonstrate that the Raman-induced SSFS plays a central role in these propagation dynamics, which makes it possible for a soliton to tunnel across the spectrally limited region of normal GVD[9–12]. The SST effect is also considered as one kind of the soliton-induced DW generation, since the transferred soliton is phase-matched to the launched soliton. Moreover, the group-velocity matching (GVM) between the launched soliton and the transferred soliton is another necessary condition for the emergence of the SST effect[8,9]. Furthermore, a fiber with a limited normal GVD region sandwiched between two anomalous ones is required for the generation of SST. When an ultrashort pulse propagates in such a fiber, higher-order nonlinear effects such as the self-steepening (SS) effect and Raman scattering influence their spectra and shapes[6,13,14]. The strong nonlinearity of a photonic crystal fiber (PCF) makes the SS significantly affect the propagation of high-order solitons. On one hand, the SS is due to the intensity dependence of the group velocity. This forces the peak of the pulse to travel slower than the wings, which causes an asymmetrical spectral broadening of the pulse. On the other hand, the SS effect is a kind of cumulative effect with the extension of transmission distance making it stronger. That is, the asymmetrical broadening effect of the SS effect on the spectrum will become more and more remarkable[1,3]. Moreover, the SS effect and Raman scattering can form new instability regions, providing a new way for generating solitons or ultrashort pulses[15–17]. Based on the above theoretical works, we qualitatively discuss the impact of

the SS effect on SST. When a femtosecond pulse is launched in the anomalous dispersion regime, new features are revealed. It is encouraging to observe the impacts of the SS effect on SST, a case that is not previously explored. In our simulation, the numerical investigation about the SS impact on the SST in the PCF with three ZDWs is performed. We find that the SS results in the energy redistribution and also leads to the suppressing of the SSFS to a certain extent, which can impact the spectrum broadening induced by self-phase modulation (SPM). Increasing the SS coefficient will augment the peak of the red-shift spectrum and widen the blue-shift spectrum component; thereby, the new soliton forms in a long wavelength anomalous dispersion region with higher energy. As a result, the SST effect can take place in a more distinct way.

Nonlinear pulse propagation in PCFs is described by the generalized NLSE, which defines every term of nonlinear effects clearly and suitably to present a numerical research finding of the SS effect:

$$\frac{\partial U}{\partial z} = \sum_{k\geq 2} \frac{i^{k+1}\beta_k}{k!\,T_0^k} \cdot \frac{\partial^k U}{\partial \tau^k} + i\gamma P_0 \left[|U|^2 U + is\frac{\partial}{\partial \tau}(|U|^2 U) - \tau_R U \frac{\partial |U|^2}{\partial \tau} \right]. \quad (1)$$

Equation (1) is numerically solved by means of the split-step Fourier transform. Here, U and T_0 are a normalized amplitude and a time normalized parameter to the input pulse width, respectively. β_k is the kth-order dispersion coefficient at the central frequency ω_0, Z is the transmission distance along the fiber, and τ is the time in a reference frame moving with the group velocity of the pulse; on the right side of Eq. (1), the dispersion effects are described by the first term, while optical nonlinear effects, such as SPM, Raman scattering, and the SS effect correspond to the second one. Dispersion parameters correspond to the polynomial that fits an order of 10 to reach a good interpolation of the dispersion profile of the PCF. The SS parameter S is $S = 1/(\omega_0 T_0)$[1,3,13]. In the numerical simulation, only a short length of the PCF is considered; for a physical understanding of the effects, the fiber loss is neglected. The injected pulse that we have adopted is the unchirped hyperbolic-secant pulse: $U(0, T) = \sqrt{P_0}\mathrm{sech}(T/T_0)$.

As mentioned before, a fiber that has a narrow normal GVD region sandwiched between two regions of anomalous GVD is required for the generation of SST. In this Letter, the three ZDWs ($\lambda_1 < \lambda_2 < \lambda_3$) of the adopted PCF are located at 771, 924, and 1014 nm, respectively[18], which divides the entire spectrum into four parts [short wavelength normal dispersion region (D1: $\lambda < \lambda_1$), short wavelength anomalous dispersion region (D2: $\lambda_1 \leq \lambda \leq \lambda_2$), long wavelength normal dispersion region (D3: $\lambda_2 \leq \lambda \leq \lambda_3$), long wavelength anomalous dispersion region (D4: $\lambda > \lambda_3$)], as shown in Fig. 1(a). The dispersion parameter curve and the relative group delay curve are

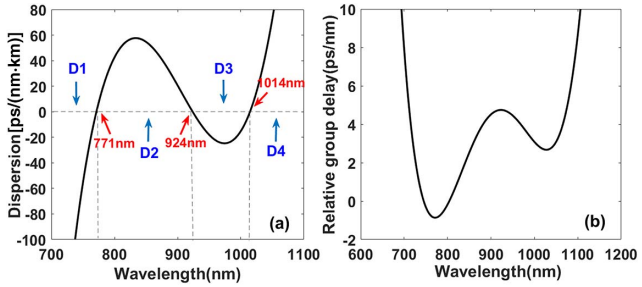

Fig. 1. (a) Curve of the dispersion parameter. (b) Curve of relative group delay.

presented in Fig. 1. Besides, the fiber's nonlinear parameter is $\gamma = 0.126\ \mathrm{W}^{-1}\cdot\mathrm{m}^{-1}$, and the part of the Raman response contribution is f_R with the value typically set to 0.18 in the PCF. The input pulse parameters in our simulation experiment were used as follows: the pump wavelength $\lambda_0 = 804$ nm, the fiber length is 60 cm, and the peak power $P_0 = 200$ W.

The SS parameter is adjusted by changing the initial pulse width in a limited range from 105 to 85 fs, but the carrier frequency ω_0 is fixed to ensure that the dispersion parameter β_k remains the same. Moreover, it is also worthy to note that the spectral width of the input pulse satisfies the condition $\Delta\omega \ll \omega_0$ to ensure that Eq. (1) is always applicable when changing the initial pulse width in our numerical simulations.

Provided that a large spectral overlap exists, the pump efficiently sheds energy away to the DW in the normal dispersion region of the PCF. The center frequencies of the DW are determined by the phase-matching (PM) condition[1,19,20]:

$$\Delta\beta = \beta(\omega_P) - \beta(\omega_{\mathrm{DW}}) = (1 - f_R)\gamma(\omega_P)P_P - \sum_{n\geq 2}^{n=10} \frac{\omega_{\mathrm{DW}} - \omega_P}{n!}\beta_n(\omega_P) = 0, \quad (2)$$

where $\beta(\omega_{\mathrm{DW}})$ and $\beta(\omega_P)$, respectively, represent the propagation constants at the angular frequency of the DWs ω_{DW} and the pump ω_P. P_P is the peak power of the pump pulse. When the soliton propagates in the anomalous dispersion regime, if $\beta_3 > 0$, the blue-shifted DW (B-DW) is generated at the short wavelength of the spectrum. In contrast, for $\beta_3 < 0$, the red-shifted DW (R-DW) is generated at the short wavelength of the spectrum. DWs as soliton-induced optical Cherenkov radiation are resonant waves meeting the PM condition with the launched soliton. Simultaneously, DWs play a crucial role in the generation and evolution of the SC in the fiber structures, since they dominate the blue-shifted edge of the spectrum, while Raman-induced SSFS results in the red-shifted edge[21]. Such a mechanism has been theoretically and experimentally demonstrated in the PCF with two or three ZDWs[13,20]. Because the interaction between the DW and soliton is a complicated nonlinear

process, we analyze the SST phenomenon by numerical simulation.

In order to understand the influence of the SS coefficient on the SST effect, we first show the spectral evolution of input pulses propagating through the 60 cm PCF with the different SS coefficients in Fig. 2. As shown in Fig. 2, the spectral intensity using a logarithmic density scale is truncated at 50 dB. In the initial stage of spectral evolution, the symmetrical spectrum broadening and pulse compression are initiated by SPM. Optical pulses generally transmit in the form of high-order solitons in the anomalous dispersion region of the fiber, especially ultrashort pulses. However, these solitons are easily affected by the high-order dispersion and nonlinear effect, and meanwhile outwardly radiate energy in the form of non-soliton radiation to sustain the soliton wave[22,23]. As indicated by Fig. 2, the injected pulse attains its maximum bandwidth after strong temporal compression and then evolves through the perturbations of high-order dispersion and other nonlinear effects, such as stimulated Raman scattering (SRS) and four-wave mixing (FWM), where the high-order soliton begins to split into a series of fundamental solitons with different peak intensities in D2[24–27]. In this process, according to the PM condition between the soliton and the DWs, the soliton can respectively radiate B-DW and R-DW to the normal dispersion region on both sides[28–30]. After the initial fission, due to the effect of RIFS, the fundamental solitons ejected in D2 undergo a continuous red-shift to the longer wavelength region with respect to the incident pulse. The soliton that is first ejected has the shortest pulse width and the strongest peak power, experiences greater frequency downshifts, and plays a major role in the process of producing dispersion waves. With further transmission in the fiber, an obvious phenomenon of the efficient energy conversion between the soliton and R-DW was observed; the DW that is radiated in

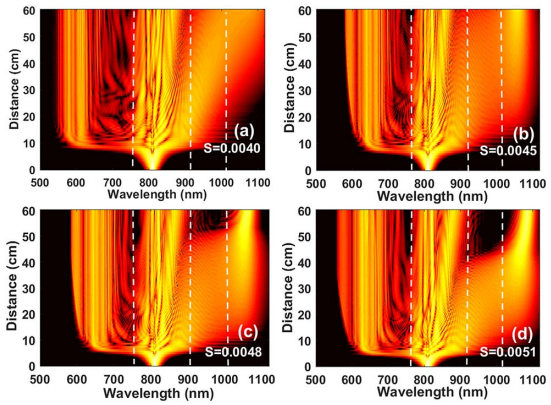

Fig. 2. Evolution of the spectral characteristic as a function of fiber length pumped at 804 nm with different SS coefficients: (a) $S = 0.0040$, (b) $S = 0.0045$, (c) $S = 0.0048$, and (d) $S = 0.0051$. The vertical dashed lines mark the three ZDWs of the fiber, separating regions D1, D2, D3, and D4, in which the normal GVD region D3 is sandwiched by two anomalous ones, D2 and D4.

the low-frequency anomalous dispersion region still transmits in the form of a soliton low-frequency anomalous dispersion wave, and the soliton in D4 of the low-frequency region is called a red-shifted soliton (R-S) here. As shown in Figs. 2(a) to 2(d), the R-DWs appear, and they are amplified when the solitons gradually shift to the second ZDW. With the increasing SS coefficient, the suppression of SSFS leads to the Raman soliton staying much longer at the blue side, so the intensity of B-DWs is strengthened to a small extent, while the energy intensity of the R-DWs in D3 declines slightly. This feature indicates that the SS effect can make energy redistribution between DWs and solitons. On the other hand, we observed that the injected pulse reaches the fission stage earlier, and the R-DWs are excited at a shorter propagation distance. Although energy intensity of the R-DWs in D3 declines slightly on account of the suppression on the SSFS, the R-S in D4 is generated with more concentrated energy at the shorter transmission distance, resulting in a more distinct SST effect, as seen in Fig. 2(d).

From the spectral evolution in Fig. 2(a), the initial pulse undergoes broadening within about 8 cm, and then breaks up into a series of fundamental solitons, accompanied by the emission of the associated DWs. On the basis of the PM condition, while the D2's fundamental soliton undergoes strong RIFS and red-shifts to the second ZDW, the energy is continually transferring from D2 to the low-frequency dispersion region at the output of the PCF, but does not take the form of the conventional fundamental soliton, which indicates that the new soliton has not yet been fully generated in D4. Thereby, the SST effect does not occur within the 60 cm propagation distance under this condition. In Fig. 2(b), the pulse reaches the fission stage at about 5 cm. The Raman solitons in D2 tunnel across a spectrally limited region of the normal GVD (D3) by transferring the energy to the R-DW; meanwhile, the R-DW in D3 also transfers the energy to the R-S in D4. Subsequently, we can observe that the soliton is formed at about 50 cm due to the SPM, which leads to the delicate balance between dispersive broadening, and nonlinear compression leads to the generation of the R-S in D4. Besides, the R-S suddenly ceases to shift on account of the balance between the SSFS and the effect of spectral recoil. However, the gathered energy of R-S in D4 is relatively faint, so that the SST effect is not particularly noticeable. With the increase of SS, as shown in Figs. 2(b)–2(d), the intensities of the R-S in D4 and the related B-DWs in D1 are enhanced, while the intensities of R-DWs in D3 fade. Because the increasing SS effect makes the incident pulse split earlier, in the meantime, it augments the peak of the red-shift spectrum and spreads the blue-shift spectrum component. In Fig. 2(d), the R-S is generated at 40 cm, and the energy of the R-S increases significantly, while most of the energy of the fundamental soliton is fully coupled into D4. More importantly, when the GVM condition between fundamental solitons and DWs is satisfied, fundamental solitons can capture the B-DWs at the forefront under the effect of FWM, and

the intensity of the captured B-DW is associated with the intensity of the fundamental soliton formed in D4.

Comparing Figs. 2(b) and 2(c) with 2(d), as the SS coefficient increases, the intensity of the R-S is sharply enhanced, and the SST becomes much more evident. Simultaneously, the intensity of B-DWs is slightly enhanced. In order to make a more accurate presentation on how the intensity of the B-DW and R-S changes over a range of SS coefficients, we plot Fig. 3, and the evolution of the power ratio of the B-DWs and R-S with respect to the entire output spectral power is plotted as a function of the SS coefficient in the figure. By conducting high-density and uniform sampling on the energy of the output spectrum at the 60 cm transmission distance, the energy ratio of the R-S in D4 to total output spectrum can be approximately calculated, and the transfer ratio of energy is formulated as $\eta = E_{\mathrm{DW}}/E_{\mathrm{TOTAL}}$. We can clearly see that the intensity of the R-S is significantly affected by the SS in a wide range of values. As the SS coefficient increased from 0.0040 to 0.0051, the percentage of the power ratio of the R-S is appreciably enhanced, and the figure grows dramatically from 5% to 21%. When the value of the SS is 0.0051, the R-DWs in D3 transfer almost all of its energy to the R-S in D4. Furthermore, while the B-DWs change relatively slightly, there is a slow growth in the percentage of B-DWs' power ratio from 32% to 35%. These results indicate that the SS effect can bring about the energy redistribution between DWs and solitons; the power ratio of R-S is enhanced significantly, and the power ratio of B-DWs is also enhanced slightly just as we have discussed for Fig. 2.

Figure 4 shows the corresponding numerical cross-correlation frequency-resolved optical grating (X-FROG) trace, which simultaneously describes the spectral and temporal content of the signal at the end of the fiber. We can observe that the change of optical spectrum tunneling is more evident. For $S = 0.0040$ in Fig. 4(a), it is evident that there is an elongated wave in the long wavelength position that is actually not a frequency-locked soliton wave, but just a leakage-like DW, which indicates that the SST did not appear, and the phenomenon

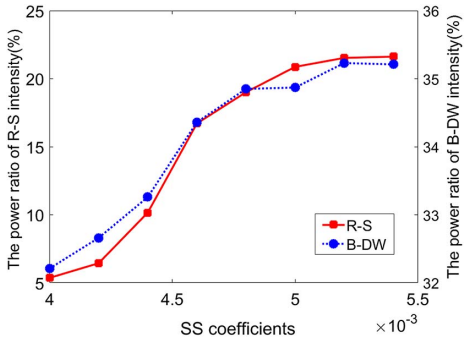

Fig. 3. Conversion efficiency of the energy contained in the R-S (red square, symbol line) and B-DWs (blue circles, symbol line); DWs along the length of the PCF are plotted as a function of the SS coefficient.

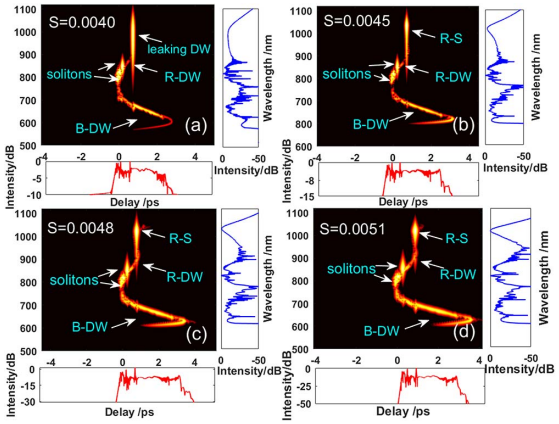

Fig. 4. Time-frequency diagram at the output of the 60 cm PCF length for (a) $S = 0.0040$, (b) $S = 0.0045$, (c) $S = 0.0048$, and (d) $S = 0.0051$, respectively.

is consistent with that in Fig. 2(a). While the SS coefficient increases from 0.0040 to 0.0051, we can see from Fig. 4 that the energy of R-S, which sheds from the Raman solitons and R-DWs, increases about 18%, and the energy in the long wavelength normal dispersion region D3 gradually reduces, accompanied by energy continuously transferring to the R-S. For $S = 0.0051$ in Fig. 4(d), ultimately almost all of the energy in D3 is transferred to the R-S in D4, and the spectrum intensity of the long wavelength anomalous dispersion region D4 has a gradually increasing peak shape at about 1069 nm, where it is obvious that the SST effect appears. Simultaneously, the energy of B-DWs in D1 increases a little. In this case, the prerequisite for the energy transferred from the Raman solitons and R-DWs to the R-S is given by the superposition of the soliton spectrum with the spectral region that is initiated by the PM condition. The energy transfer rate can be manipulated by the initial SS coefficient of the pulse. Therefore, efficient conversion of energy among the spectral components can be acquired.

To clearly show the generation of the SST effect along with the pulse evolution process, Fig. 5 shows corresponding numerical X-FROG traces of femtosecond pulses at six different distances in the PCF with three ZDWs. For $S = 0.0051$ in Fig. 5(a), at the beginning of the propagation distances from 0 to 5 cm, the spectrum is broadened symmetrically due to the influence of SPM. With further transmission at the slightly longer propagation distance between 5 and 15 cm, the SPM dominated stage of the SC development ends, and the high-order soliton begins to split up. Due to the influence of the SS effect and other terms of nonlinear effects, the spectrum is broadened asymmetrically, as seen in Fig. 5(b)[31]. In Fig. 5(c), owing to the PM condition, D2's soliton radiates B-DW in D1 and R-DW with low intensity in D3. Figure 5(d) shows Raman solitons gradually red-shift to the long wavelength position by the effect of RIFS. When the Raman soliton steadily approaches the second ZDW, it radiates R-DWs to the long wavelength region[32,33]. When the pulse

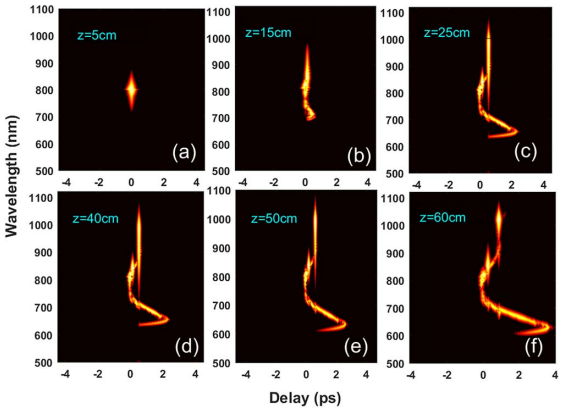

Fig. 5. Numerical X-FROG traces of the pulse for different propagation lengths z. (a) $z = 5$ cm, (b) $z = 15$ cm, (c) $z = 25$ cm, (d) $z = 40$ cm, (e) $z = 50$ cm, and (f) $z = 60$ cm for $S = 0.0051$.

propagates from 40 to 60 cm, the energy continuously shifts toward D4 from the solitons in D2 and the R-DWs in D3, where the R-S gradually takes shape in D4. As seen in Fig. 5(f), the energy intensity of the R-S in D4 is gradually focused. Eventually the fundamental solitons tunnel across the forbidden region of normal dispersion D3 and form a new soliton in D4, and the SST effect is unusually distinct. It is in this way that the SST effect can be produced to reshape the spectrum and provide a mechanism for pulse compression.

In this Letter, the impact of the SS effect on SST during the process of SCG in the PCF with three ZDWs is investigated numerically, the spectrum evolution in the process of pulse propagation is simulated, and the analysis about the time-frequency characteristics of output pulse in different SS coefficients is given. Our results show that the SS induces the redistribution of spectrum energy, and the SST effect is appreciably affected by the SS effect. As the SS coefficient increases, the peak of the red-shift spectrum is enhanced, and the blue-shift spectrum component is broadened, where more energy transfers from the solitons in D2 and R-DW in D3 to the R-S generated in D4. Consequently, the R-S forms at a shorter distance and has a higher energy accumulation, which makes the SST effect more obvious, contributing to the reshaping of the SC. Furthermore, the enhanced energy of B-DWs can extend the blue edge of the SC. Therefore, the simulation and analysis presented here may open up the possibility of generating and reshaping the SST effect in the PCF; it is possible to obtain a high-power spectral component at flexible wavelengths, which shapes the SC spectrum uniquely and allows for the redistribution of pump energy with high efficiency. It has potential applications in ultra-short pulse compression, optical sensing, or certain novel applications in nonlinear optics, but also has great research value in optical soliton dynamics, while simultaneously giving more value for the PCF with three ZDWs in physical applications.

This work was supported by the National Natural Science Foundation of China (Nos. 61275137 and 61571186) and the Natural Science Foundation of Hunan Province of China (No. 2018JJ2061).

References

1. J. M. Dudley, G. Genty, and S. Coen, Rev. Mod. Phys. **78**, 1135 (2006).
2. M. A. Foster, A. C. Turner, M. Lipson, and A. L. Gaeta, Opt. Express **16**, 1300 (2008).
3. G. P. Agrawal, *Nonlinear Fiber Optics*, 4th ed. (Academic, 2007).
4. S. Zhao, H. Yang, C. Zhao, and Y. Xiao, Opt. Express **25**, 7192 (2017).
5. X. Feng, F. Poletti, A. Camerlingo, F. Parmigiani, P. Petropoulos, P. Horak, G. M. Ponzo, M. Petrovich, J. Shi, W. H. Loh, and D. J. Richardson, Opt. Fiber. Technol. **16**, 378 (2010).
6. A. Mahalingam and M. S. Mani Rajan, Opt. Fiber. Technol. **25**, 44 (2015).
7. B. Kibler, P. A. Lacourt, F. Courvoisier, and J. M. Dudley, Electron. Lett. **43**, 967 (2007).
8. H. Guo, S. Wang, X. Zeng, and M. Bache, IEEE Photon. Tech. Lett. **25**, 1928 (2013).
9. F. Poletti, P. Horak, and D. J. Richardson, IEEE Photon. Technol. Lett. **20**, 1414 (2008).
10. V. N. Serkin and T. L. Belyaeva, J. Express Theor. Phys. Lett. **74**, 573 (2001).
11. A. C. Newell and J. Math, J. Math. Phys. **19**, 1126 (1978).
12. J. F. Wang, L. Li, and S. T. Jia, J. Opt. Soc. **25**, 1254 (2008).
13. B. Kibler, P. A. Lacourt, F. Courvoisier, and J. M. Dudley, Electron. Lett. **43**, 967 (2007).
14. V. N. Serkin, V. A. Vysloukh, and J. R. Taylor, Electron. Lett. **29**, 12 (1993).
15. H. Yang, B. Wang, N. Chen, X. Tong, and S. Zhao, Opt. Commun. **359**, 20 (2016).
16. D. V. Skryabin and A. V. Gorbach, Rev. Mod. Phys. **82**, 1287 (2010).
17. C. Dai, H. Zhu, and C. Zheng, Z. Naturforsch. **67**, 338 (2012).
18. Z. Hao, C. Zhao, J. Wen, S. Wen, and D. Fan, Acta. Opt. Sin. **31**, 1006003 (2011).
19. S. Zhao, H. Yang, N. Chen, and C. Zhao, Sci. Rep. **7**, 39926 (2017).
20. W. Wang, H. Yang, P. Tang, C. Zhao, and J. Gao, Opt. Express **21**, 11215 (2013).
21. S. Vyas, T. Tanabe, M. Tiwari, and G. Singh, Chin. Opt. Lett. **14**, 123201 (2016).
22. P. Maji and R. Das, Chin. Opt. Lett. **15**, 070606 (2017).
23. J. Wang, Z. Jiang, H. Chen, J. Li, J. Yin, J. Wang, T. He, P. Yan, and S. Ruan, Photon. Res. **6**, 535 (2018).
24. C. R. Petersen, U. Møller, I. Kubat, B. Zhou, S. Dupont, J. Ramsay, T. Benson, S. Sujecki, N. Abdel-Moneim, Z. Tang, D. Furniss, A. Seddon, and O. Bang, Nat. Photon. **8**, 830 (2014).
25. S. Zhao, H. Yang, N. Chen, and C. Zhao, IEEE Photon. J. **7**, 7102701 (2015).
26. H. Qin and X Xiao, Chin. Opt. Lett. **15**, 030604 (2017).
27. M. Klimczak, B. Siwicki, A. Heidt, and R. Buczyński, Photon. Res. **5**, 710 (2017).
28. E. N. Tsoy and M. De Sterke, Phys. Rev. **76**, 043804 (2007).
29. B. H. Chapman, J. C. Travers, S. V. Popov, A. Mussot, and A. Kudlinski, Opt. Express **18**, 24729 (2010).
30. H. Yang, Q. Zeng, H. Hu, B. Wang, and W. Wang, Opt. Commun. **325**, 170 (2014).
31. L. He, B. Yang, X. Zhang, and L. Yu, Chin. Opt. Lett. **4**, 715 (2006).
32. H. Chen, Z. Chen, X. Zhou, and J. Hou, Chin. Opt. Lett. **10**, 120603 (2012).
33. S. Wang, H. Guo, D. Fan, X. Bai, and X. Zeng, IEEE Photon. **5**, 6100608 (2013).